

Journal Pre-proof

Design-based synthesis, molecular docking analysis of an anti-inflammatory drug, and geometrical optimization and interaction energy studies of an indole acetamide derivative

Fares Hezam Al-Ostoot, D.V. Geetha, Yasser Hussein Eissa Mohammed, P. Akhileshwari, M.A. Sridhar, Shaukath Ara Khanum

PII: S0022-2860(19)31353-5

DOI: <https://doi.org/10.1016/j.molstruc.2019.127244>

Reference: MOLSTR 127244

To appear in: *Journal of Molecular Structure*

Received Date: 9 August 2019

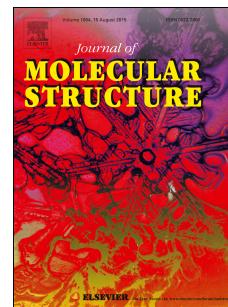
Revised Date: 18 September 2019

Accepted Date: 17 October 2019

Please cite this article as: F.H. Al-Ostoot, D.V. Geetha, Y.H.E. Mohammed, P. Akhileshwari, M.A. Sridhar, S.A. Khanum, Design-based synthesis, molecular docking analysis of an anti-inflammatory drug, and geometrical optimization and interaction energy studies of an indole acetamide derivative, *Journal of Molecular Structure* (2019), doi: <https://doi.org/10.1016/j.molstruc.2019.127244>.

This is a PDF file of an article that has undergone enhancements after acceptance, such as the addition of a cover page and metadata, and formatting for readability, but it is not yet the definitive version of record. This version will undergo additional copyediting, typesetting and review before it is published in its final form, but we are providing this version to give early visibility of the article. Please note that, during the production process, errors may be discovered which could affect the content, and all legal disclaimers that apply to the journal pertain.

© 2019 Published by Elsevier B.V.



Design-based synthesis, molecular docking analysis of an anti-inflammatory drug, and geometrical optimization and interaction energy studies of an indole acetamide derivative

Authors: Fares Hezam Al-Ostoot^{1,2}, Geetha D. V.³, Yasser Hussein Eissa Mohammed⁴, Akhileshwari P.³, Sridhar M. A.^{3*}, Shaukath Ara Khanum¹

Affiliations:

¹Department of Chemistry, Yuvaraja's College, University of Mysore, Mysuru 570 006, India.

²Department of Biochemistry, Faculty of Education & Science, Al-Baydha University, Yemen.

³Department of Studies in Physics, Manasagangotri, University of Mysore, Mysuru 570 006, India.

⁴Department of Biochemistry, Faculty of Applied Science, University of Hajjah, Yemen.

* Correspondence should be addressed to *Dr. Sridhar M. A.*,

Email: *mas@physics.uni-mysore.ac.in*

Dr. Sridhar M. A.

Professor

Department of Studies in Physics

Manasagangotri

University of Mysore

Mysuru 570 006

India

Tel: 0821 2419333

Abstract

The new indole acetamide, *N*-(2-(2-(4-Chlorophenoxy)acetamido)phenyl)-2-carboxamide-1*H*-indole (**5**) has been synthesized with good yield by stirring the compound *N*-(2-Aminophenyl)-2-(4-chlorophenoxy)acetamide (**3**) with 1*H*-indole-2-carboxylic acid (**4**), in dry dichloromethane (DCM) followed by the addition of lutidine, and *N,N,N',N'*-O-(Benzotriazole-1-yl)-tetramethyluronium tetrafluoroborate (TBTU) in cooled condition. The compound obtained was characterized by spectroscopic analyses (MS, FT-IR, ¹H NMR, ¹³C NMR, UV-visible, and elemental). The anti-inflammatory activity was confirmed by *in silico* modeling study, which target the cyclooxygenase COX-1 and 2 domains. The three-dimensional structure was determined using single crystal X-ray diffraction studies. Geometry optimization of the compound was done using density functional theory calculations by employing B3LYP hybrid functional basis set. Vibrational analysis of the compound revealed that the optimized structure is not in an excited state. Frontier molecular orbitals Highest Occupied Molecular Orbital (HOMO) and lowest Unoccupied Molecular Orbital (LUMO) were analyzed to understand the electronic charge transfer within the molecule. To analyze the intermolecular interactions in the crystal, Hirshfeld surface analysis was carried out. Energy frameworks were constructed to investigate the stability of the compound. Atom in molecule (AIM) calculations were performed to validate the different intramolecular interactions.

Keywords: Anti-inflammatory, docking studies, DFT, Hirshfeld surface analysis, HOMO, LUMO, AIM.

1. Introduction

Fever, swelling, and pain are some aspects of the inflammation which is a defense mechanism produced by prostaglandins aimed to protect the body from infections or any physical or chemical danger [1]. This defense mechanism also acts against life-threatening conditions which include autoimmune diseases like rheumatoid arthritis and inflammatory intestinal syndrome [2]. There have been two forms identified of COX which are COX-1 and COX-2. In 2002, a third one COX-3 was discovered. In the gastrointestinal tract, the cytoprotection effect is provided by COX-1 while the inflammation is mediated by COX-2 [3]. In palliative care, the non-steroidal anti-inflammatory medicines (NSAIDs) are widely used as efficient analgesics. However, the prolonged use of these drugs can lead to serious side effects such as gastric irritation, ulceration or bleeding [4]. Indomethacin, for example, is an indole derivative and NSAID drug known to cause ulcers for its users, but it's undergoing chemical modification to make it safer for use [5]. This has shown, that synthesis of

derivatives with significant anti-inflammatory activity and fewer side effects of chemical modification has a high possibility which encouraged us to synthesized newer derivatives of heterocyclic indole aiming to obtain better inflammatory agents with fewer side effects.

In drug discovery, medicinal chemists use the privileged structures (PS) to synthesize novel compounds based on a central scaffold, and screen them against different receptors involved in various pathways, producing biologically active compounds. Indole nucleus as a unique template is often found in the medicinal chemistry domain with wonderful properties due to the presence of a rich in electron pyrrole moiety [6, 7] that can use non-covalent interactions with other molecules by the formation of hydrogen bonding in the NH moiety by π - π system [8] and is considered as PS [9]. Due to this inimitable property, indole and its various derivatives are used broadly for drug design and development [10]. Therefore, it has highlighted considerable attention to the development of synthetic methods and the elucidation of its pharmaceutical properties for applications including: an anti-inflammatory [11-15] cardiovascular [16] anti-histaminic [17, 18], anti-oxidant [19], anti-rheumatoid, anti-HIV [20, 21] and anti-cancer activity [22-25] which probably refer to compounds bearing indole moiety. Indole and its derivatives also play a vital role in the immune system [26, 27].

Further, it is considered as the most potent scavenger of free radicals [28]. Different studies involving *in vitro* and *in vivo* inhibition activities have shown that compounds with indole moiety can effectively inhibit the diabetic activity [29]. Therefore, the design and selective functioning of indole have been the center of the current investigation over the years [30, 31]. In view of their broad spectrum of biological properties and as a part of our ongoing work on synthesis and characterization of indole and acetamide derivatives [32-35]. The compound was synthesized and characterized spectroscopically and the molecular structure was confirmed by single crystal X-ray diffraction studies. In addition, computational biology and bio-informatics have the potential of not only speeding up the drug discovery process, but also about changing the way drugs are designed and thus, reducing the costs. Rational drug design helps to facilitate and speed up the drug designing process, which involves a variety of methods to identify novel compounds. One such method is the docking of the drug molecule with a receptor.

The compound *N*-(2-(2-(4-Chlorophenoxy)acetamido)phenyl)-2-carboxamide-1*H*-indole is an indole derivative. In the present study, we report the theoretical and experimental investigations of the compound by employing Density Functional Theory (DFT), Hirshfeld surface analysis, and molecular

docking tools. DFT has become an important tool in modern quantum computational chemistry to explain the various electronic transitions and chemical properties of the compound. The optimized molecular properties with DFT approach admit a close connection between theoretical and experimental results. DFT calculations depend on the electron density distribution function of the compound being studied. The frontier molecular orbitals HOMO and LUMO and their energy gaps were analyzed. Vibrational frequency analysis was done to know the various normal mode frequencies.

2. Materials and methods

2.1. Experimental section

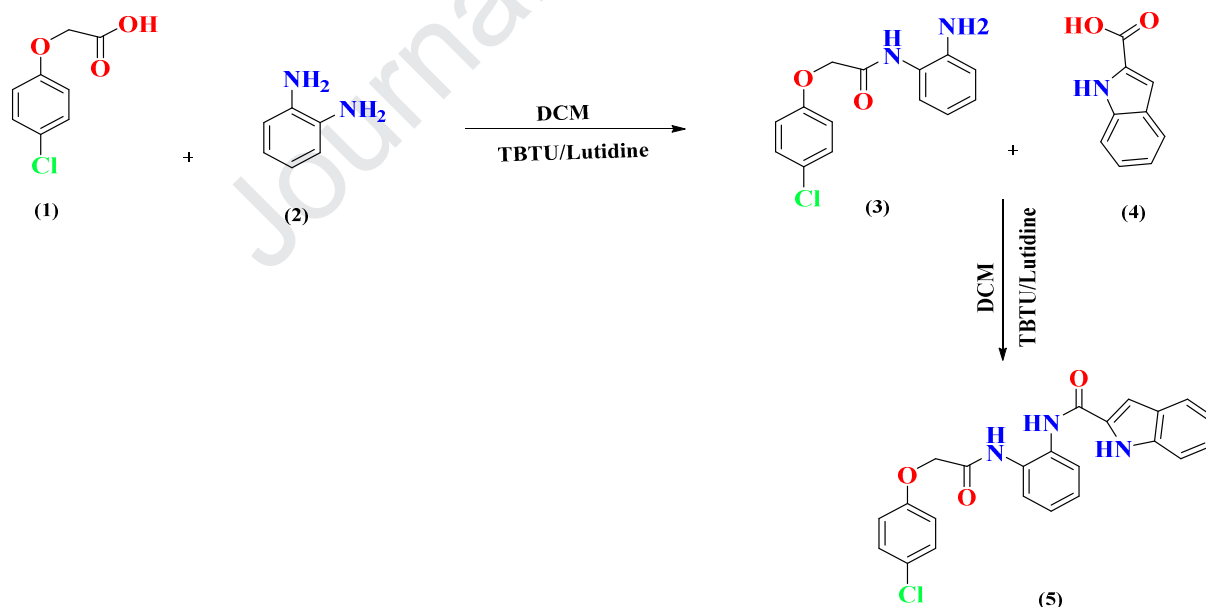
Chemicals, solvents and agents were purchased from Sigma Aldrich, analytical thin layer chromatography (TLC) was performed on (0.25 mm) silica gel plates (Merck 60 F₂₅₄) by using the solvent system [hexane: ethyl acetate (3:1)]. Melting point was determined using the Chemi Line CL725 Micro Controller Based melting point apparatus with a digital thermometer. ~~The purity of the compound was confirmed by thin layer chromatography using silica gel G and spots were located by iodine.~~ The IR spectrum was recorded by the potassium bromide pellet method on Cary 630 FTIR Agilent spectrophotometer, NMR spectrum was recorded on a VNMRS-400 MHz Agilent-NMR spectrophotometer in dimethyl sulfoxide (DMSO). Mass spectrum was obtained with a VG70-70H spectrometer. Elemental analysis results are within 0.5% of the calculated value.

Synthesis of *N*-(2-Aminophenyl)-2-(4-chlorophenoxy)acetamide (**3**)

The title compound *N*-(2-Aminophenyl)-2-(4-chlorophenoxy)acetamide (**3**), was accomplished by a synthetic procedure as shown in **scheme 1**. To 2-(4-chlorophenoxy) acetic acid compound (**1**, 0.009 mol), in dry DCM (10 ml), lutidine (0.02 mol.) was added at 25-30 °C, followed by the addition of 1, 2-diaminobenzene (**2**, 0.009 mol), the reaction mixture was stirred at 25-30 °C for 25 min. The reaction was cooled to 0-5 °C, TBTU (0.02 mol) was added over a period of 30 min while maintaining the temperature below 5 °C. The reaction was stirred overnight and monitored by TLC using mobile phase system [hexane: ethyl acetate (3:1)]. The reaction mixture was diluted with 25 ml of DCM and treated with 2N hydrochloric acid solution (20 ml). The organic layer was washed with water (3 × 25 ml) and brine (3 × 25 ml). Finally, the organic layer was dried over anhydrous sodium sulfate and concentrated to afford the compound (**5**) [36].

Synthesis of *N*-(2-(2-(4-Chlorophenoxy)acetamido)phenyl)-2-carboxamide-1*H*-indole (5)

To the compound of *N*-(2-Aminophenyl)-2-(4-chlorophenoxy)-acetamide (3, 0.002 mol), in dry DCM (10 ml), 1*H*-indole-2-carboxylic acid (4, 0.002 mol), was added at 25-30 °C, followed by the addition of lutidine (0.001 mol). The reaction mixture was stirred at 25-30 °C for 30 min. The reaction was cooled to 0-5 °C, TBTU (0.003 mol) was added over a period of 30 min while maintaining the temperature below 5 °C. The reaction was stirred overnight and monitored by TLC using mobile phase system of [hexane: ethyl acetate (3:1)]. The reaction mixture was diluted with (25 ml) of DCM and treated with 10% of sodium bicarbonate solution (3 x 25 ml), dried over anhydrous sodium sulfate and concentrated to yield compound (5) [37]. Then it dried to obtain a crude product which on recrystallization with ethanol afforded the title compound (5) as colorless rectangular block shape crystals, and then confirmed by NMR, LC-MS spectra (figures 2 and 3). The schematic diagram of the synthesized compound is shown in **scheme 1**.



Scheme 1: Reaction pathway for the synthesis of the title compound (5).

2.2. Spectral data

N-(2-Aminophenyl)-2-(4-chlorophenoxy)-acetamide (**3**)

Yield: 78%; M.P. 178-180 °C; ^1H NMR (400 MHz, DMSO- d_6) δ (ppm): 4.70 (s, 2H, OCH $_2$), 4.88 (s, 2H, NH), 6.57-7.54 (m, 8H, Ar-H), 9.20 (s, 1H, NH); LC-MS m/z 276 [M+], 278 [M+2]. Anal. Calcd. for $\text{C}_{14}\text{H}_{13}\text{ClN}_2\text{O}_2$ (276): C, 60.77; H, 4.74; N, 10.12. Found: C, 60.65; H, 4.63; N, 10.03 %.

N-(2-(2-(4-Chlorophenoxy)acetamido)phenyl)-2-carboxamide-1*H*-indole (**5**)

Yield: 85%; M.P. 205-207 °C; FT-IR (KBr, ν_{max} cm^{-1}), 725 (Aromatic bending), 1100 (C-O), 1630 (C=O), 3210-3320 (N-H); ^1H NMR (400 MHz, DMSO- d_6) δ (ppm): 4.71 (s, 2H, OCH $_2$), 6.89-7.77 (m, 13H, Ar-H), 9.65 (s, 1H, NH), 10.18 (s, 1H, NH), 11.83 (s, 1H, -NH indole); ^{13}C NMR (DMSO- d_6) δ : 166.96, 160.65, 156.44, 137.40, 131.51, 131.10, 130.10, 129.67, 129.48, 127.49, 126.43, 126.37, 125.83, 125.55, 124.44, 122.25, 120.48, 116.87, 116.63, 112.90, 104.70, 67.76; LC-MS m/z 419 [M+], 421 [M+2]. Anal. Calcd. for $\text{C}_{24}\text{H}_{21}\text{N}_3\text{O}_4$ (419): C, 69.39; H, 5.10; N, 10.01. Found: C, 69.31; H, 5.02; N, 9.90 %.

The FTIR spectrum of the compound (**5**) is shown in **figure 1**.

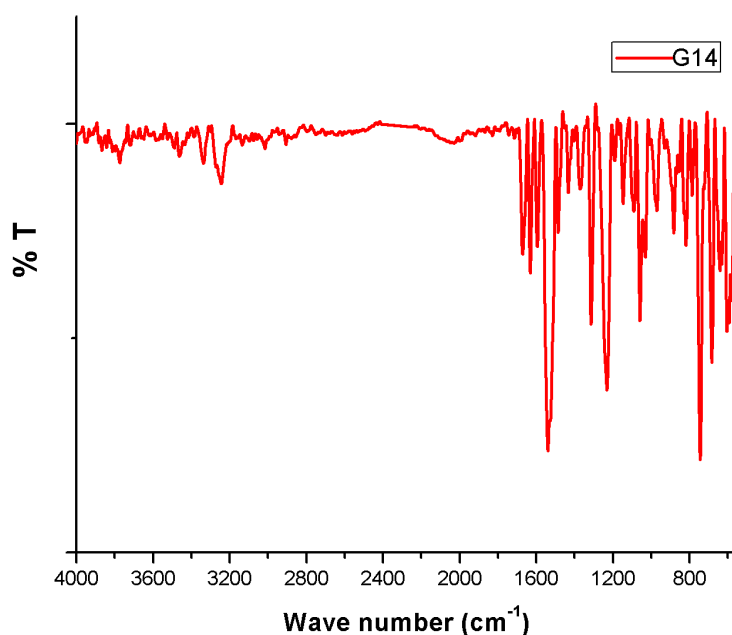


Figure 1: The FTIR spectrum of the compound (5).

Journal Pre-proof

3. Computational studies

The geometry optimization followed by vibrational analysis of the compound was carried out by density functional theory calculations using GAMESS-US software [38]. They were carried out with Becke three parameter for the exchange with correlation functional of Lee-Yang-Parr (B3LYP) for 6-31G(d,p) and 6-31+G(d,p) hybrid basis sets [39]. The frontier molecular orbitals HOMO and LUMO were investigated for the geometrically optimized structure for the same basis set levels. The Hirshfeld surface calculations were performed by employing CrystalExplorer-17 program [40]. Atom in molecule theory calculations were done by employing Multiwfn software [41].

4. Molecular docking studies of compound (5)

All the molecular docking studies were performed using Autodock software version 4.0 [42]. The standard protocol was followed to predict the binding energy and compared with the standard drug [43-45] to target the COX-1 & 2 domains. Compound (5) was selected based on structural diversity and a wide range of biological activities to study the molecular interactions involved between the active binding sites of the protein target and synthesized compound. The COX inhibitory activity of the compound (5) was ranked based on their lowest binding energy involved in the complex formation at the active sites. The binding energy of the docked compound on COX-1 and COX-2 was in the range of -7.87 and -6.77 kcal/mol, respectively. It is evident that the interaction energy of the compound (5) is lower in COX-1 than COX-2 indicating it as a COX-1 inhibitor. Several amino acid residues are involved in a particular binding mode. However, only two hydrogen bond interactions could be observed between the compound and COX-1 & 2. The carboxylic group of compound (5) forms hydrogen bonds with residues of COX-1 (SER126 and PRO125) and COX-2 (HIS386 and GLN454). Further, the interaction of the compound (5) at the pocket site and residue amino acid of the complex COX-1-(5) and complex COX-2-(5) is predicted. Hence, this compound was selected for docking studies to test the effect of the compound (5) on binding affinity to COX-1 and COX-2 in order to get a

better understanding of the effect of additional oxygen in linker chain on inhibition of COX enzyme figures 2 and 3 [46].

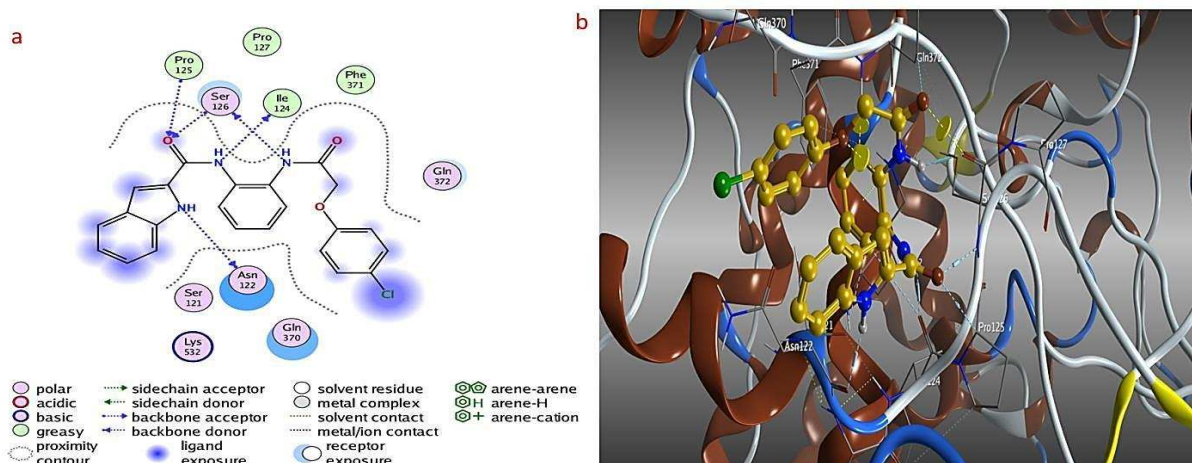


Figure 2: *In silico* interaction of compound with COX-1. **a)** 2D Interaction analysis of compound (5) with COX-1. **b)** Ribbon models of the COX-1 catalytic domain and the ligand molecule in compound (5) at the pocket site and residue amino acid at the pocket site of the COX2-(5) complex.

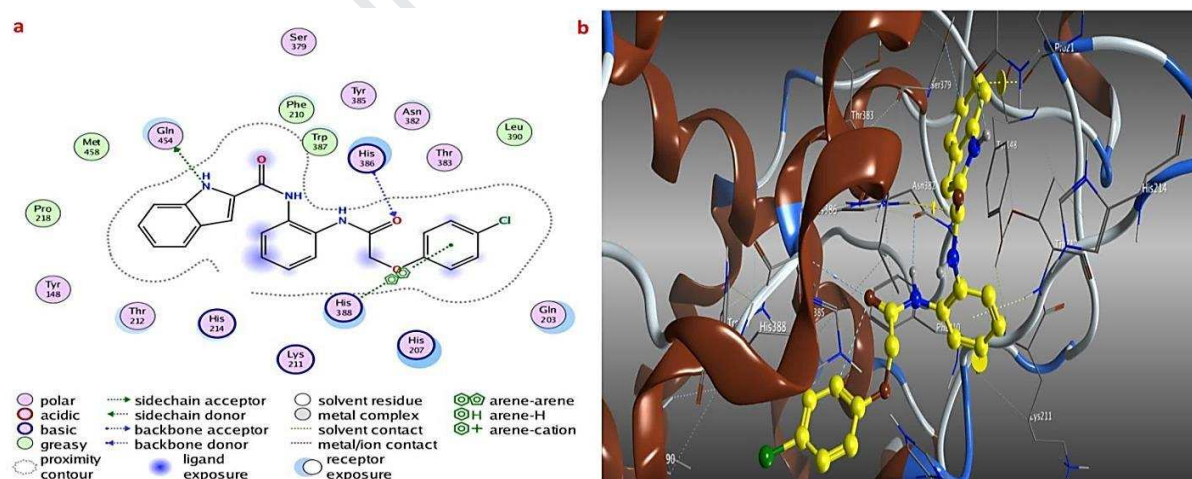


Figure 3: *In silico* interaction of compound with COX-2. **a)** 2D Interaction analysis of compound (5) with COX-2. **b)** Ribbon models of the COX-2 catalytic domain and the ligand molecule in compound (5) at the pocket site and residue amino acid at the pocket site of the COX-2-(5) complex.

5. Results and discussions

5.1 XRD and DFT calculations

From the single crystal X-ray diffraction study it is revealed that the compound (**5**) crystallizes in the monoclinic crystal system in the $P2_1/c$ space group. The geometrical parameters are: $a = 11.171(2) \text{ \AA}$, $b = 21.929(5) \text{ \AA}$, $c = 9.307(2) \text{ \AA}$, $\beta = 114.257(18)^\circ$, and volume = $2078.6(8) \text{ \AA}^3$. The *ORTEP* is shown in **figure 4** (CCDC No. 1943139).

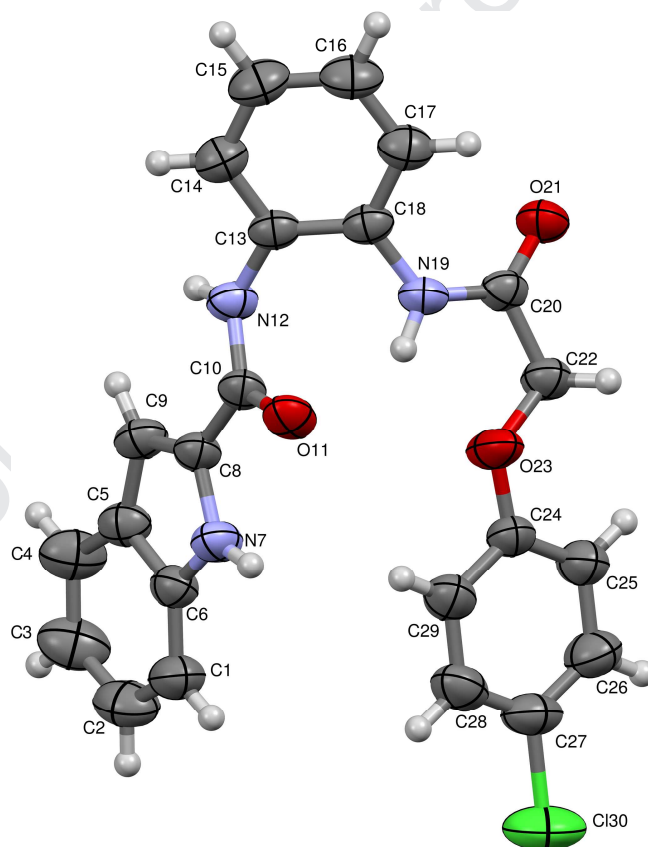


Figure 4: *ORTEP* of the molecule with thermal ellipsoids drawn at 50% probability

DFT calculations were adopted for geometry optimization. The optimized structure of the compound is shown in the **figure 5**. The bond lengths, bond angles, and torsion angles are compared with those obtained from single crystal X-ray diffraction data (refer supplementary files for the tables). The deviations in the torsion angles can be attributed to the fact that the density functional calculations

describe the molecule in the gaseous phase, whereas the experimentally obtained values are from the solid phase of the molecule.

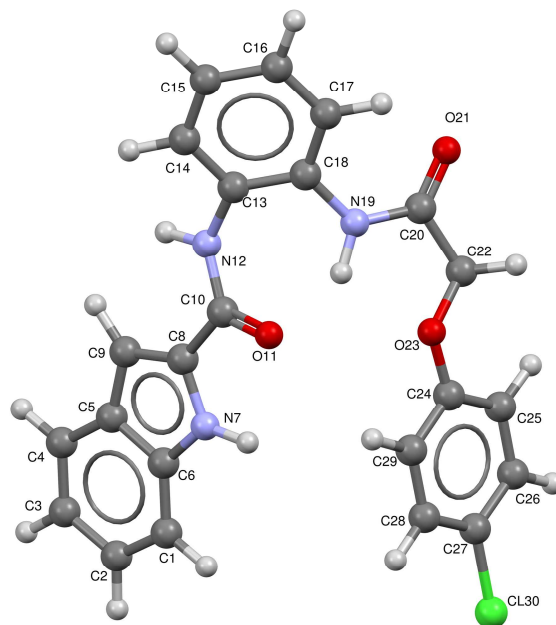
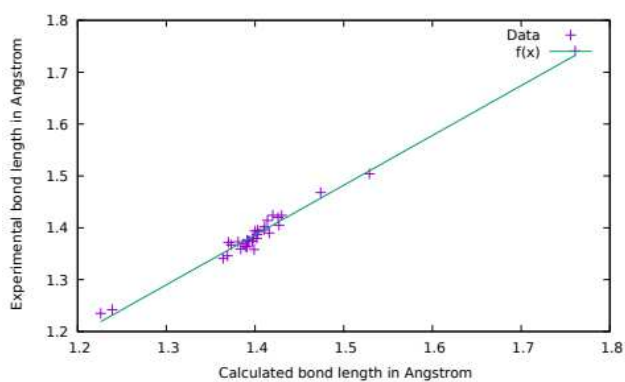
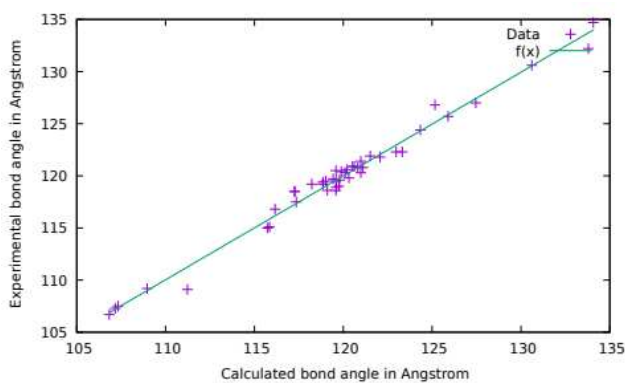


Figure 5. The optimized structure of the compound.

The graph of X-ray experimental bond length against computed bond length and X-ray bond angle against computed bond angle is plotted (**figure 6**). The plot shows better agreement with the bond length and bond angle with the correlation coefficient $R^2 = 0.982$ and $R^2 = 0.983$ respectively.



(a)



(b)

Figure 6: The correlation graph of bond lengths (a), and bond angles (b).

Root mean square deviation (RMSD) is calculated for the theoretical and experimentally obtained geometrical parameters using the expression

$$\text{RMSD} = \sqrt{\frac{1}{n-1} \left(\sum_i^n \gamma_i^{\text{cal}} - \gamma_i^{\text{exp}} \right)^2}$$

where n is the maximum number of data points. The root mean square deviation of the bond lengths, bond angles is 0.0825 Å and 0.0869 Å respectively. The vibrational frequencies of the normal modes were calculated and analyzed for the B3LYP/6-31+G(d,p) functional basis set. A total of 144 normal modes of vibrations were analyzed.

4.2 HOMO and LUMO analyses

The chemical reactivity and kinetic stability of the compound depends on the frontier molecular orbitals HOMO and LUMO. The energies between the molecular orbitals (HOMO and LUMO) including second highest occupied (HOMO-1) and second lowest unoccupied (LUMO+1) were calculated and are listed in table 4. **Figure 7** shows the HOMO LUMO energy levels for the B3LYP/6-31+G(d, p) hybrid basis set. The HOMO LUMO energies describe the electron donating and accepting ability of the molecules respectively. The gap between them, referred to as orbital energy gap, plays a vital role in determining the electron transportation capacity of the molecule. A larger gap alludes that molecule is chemically hard, stable, and unreactive; whereas a molecule with smaller orbital energy gap is soft, unstable, and reactive. It is found that the orbital energy gap for the studied compound is 4.3267 eV, which describes the partial hardness of the compound. This does not allow an easy transfer of electrons from HOMO to LUMO. The HOMO is mainly concentrated over the indole ring, while the LUMO is projected over the indole ring as well as the carbonyl group (C=O) (**figure 7**). Both HOMO and LUMO have no electron concentration in the chlorophenyl ring indicating that this ring is not participating in the intramolecular charge transfer.

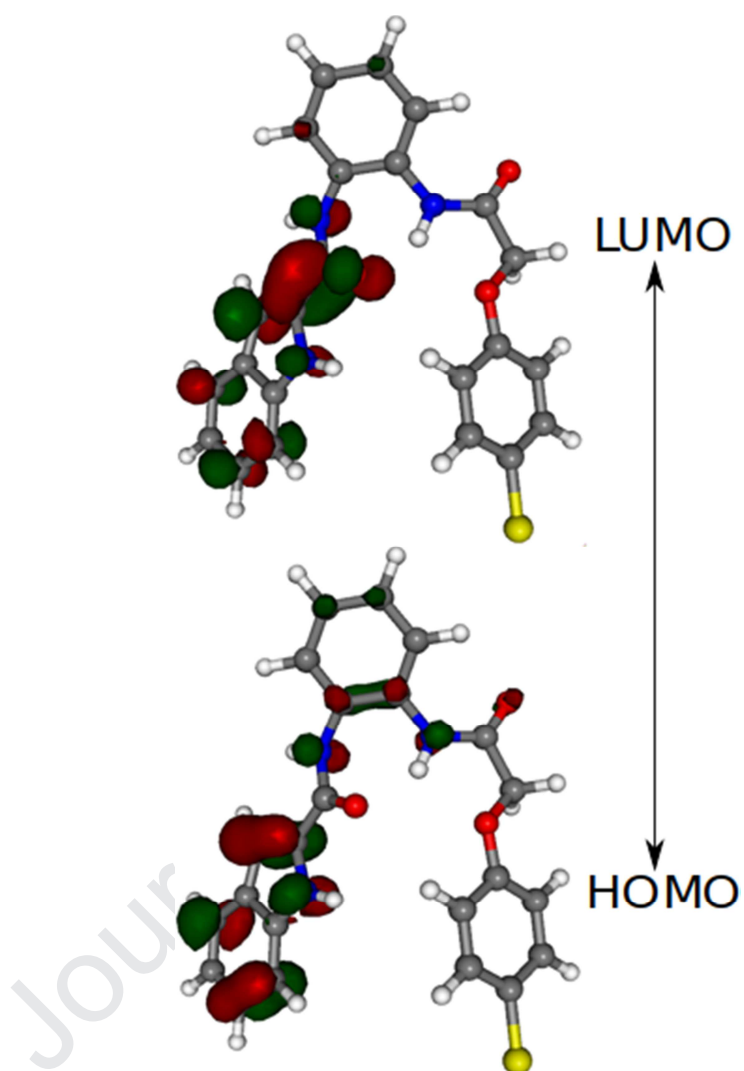


Figure 7: HOMO LUMO energy levels.

The orbital charge density isosurface value is 0.0500. The energies obtained from the HOMO and LUMO analyses can be correlated with the concerned molecular properties. Negative of HOMO energy is taken as the ionization potential; negative of LUMO energy is considered as electron affinity (EA). The average of the HOMO LUMO energies is considered as electronegativity (χ). The chemical hardness (η) is defined as half of the orbital energy gap. The calculated global descriptive parameters are listed in **table 4**.

Table 4: Calculated molecular energy values and global descriptive parameters.

Parameter	Value (eV)
E_{HOMO}	-6.1497
E_{LUMO}	-1.8230
ΔE	4.3267
$E_{\text{HOMO}-1}$	-6.3021
$E_{\text{LUMO}+1}$	-0.8620
Ionization potential (I)	6.1497
Electron affinity (A)	1.8230
Chemical potential (μ)	-3.9863
Electronegativity (χ)	3.9863
Chemical hardness (η)	2.1633

4.3 Hirshfeld surface analysis

Hirshfeld surface analysis is a tool to visualize the packing modes and intermolecular interactions in the crystal. Hirshfeld surface divides crystal space into smooth non-overlapping regions where the electron densities of a sum of spherical atoms for the molecule (promolecule) dominates the corresponding sum over the crystal (procrystal) [47, 48]. For each point on the surface, two distances d_i (distance from the Hirshfeld surface to the nucleus internal to the surface) and d_e (distance from the

Hirshfeld surface to the nucleus external to the surface) are calculated. These surfaces reflect the proximity of intermolecular interactions in the crystal. Since the computation of the d_e and d_i surfaces does not take into account the relative atomic sizes, a normalized contact distance d_{norm} is defined as

$$d_{\text{norm}} = \frac{d_i - r_i^{\text{vdw}}}{r_i^{\text{vdw}}} + \frac{d_e - r_e^{\text{vdw}}}{r_e^{\text{vdw}}},$$

where r_i^{vdw} and r_e^{vdw} are the van der Waals (vdw) radii of the atoms internal and external to the surface respectively. The various intermolecular interactions are displayed on the Hirshfeld surface by using red-white-blue color scheme. Shorter and longer intermolecular interactions (as compared to van der Waals radii) are represented by red and blue colors respectively. White color is for the contacts around van der Waals' separation [49].

The Hirshfeld surface highlights the region where the intermolecular contacts are prominent (**figure 8**). The two bright red regions seen on the Hirshfeld surface correspond to the shortest intermolecular interaction due to N-H...O contacts.

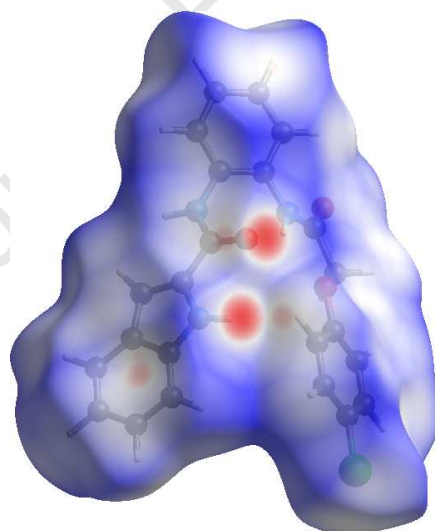


Figure 8: Hirshfeld surface mapped over d_{norm} .

4.4.1 Fingerprint plots

Fingerprint plots depict the concise summary of the 2D intermolecular interactions as well as interactions from individual contacts present in the molecular crystal. They are generated by considering d_i and d_e distances. **Figure 9** shows the fingerprint plots of the compound showing the

contribution from all the contacts and resolved into individual contacts. The strong intermolecular interactions appear as distinct spikes in the fingerprint plots. The decomposed fingerprint plot highlights the close contacts of a particular atom pair. The contributions of C-H, O-H, and Cl-H contacts to the total Hirshfeld surface area are 29.8%, 13.5%, and 10.3% respectively. The major contribution of 35.3% is from H-H contacts with $d_i + d_e \approx 2.4$ Å. The two sharp peaks observed at the top left and bottom right of the plot are from close intermolecular O-H contacts. The various C-H... π interactions appear as peripheral wings in the fingerprint plot.

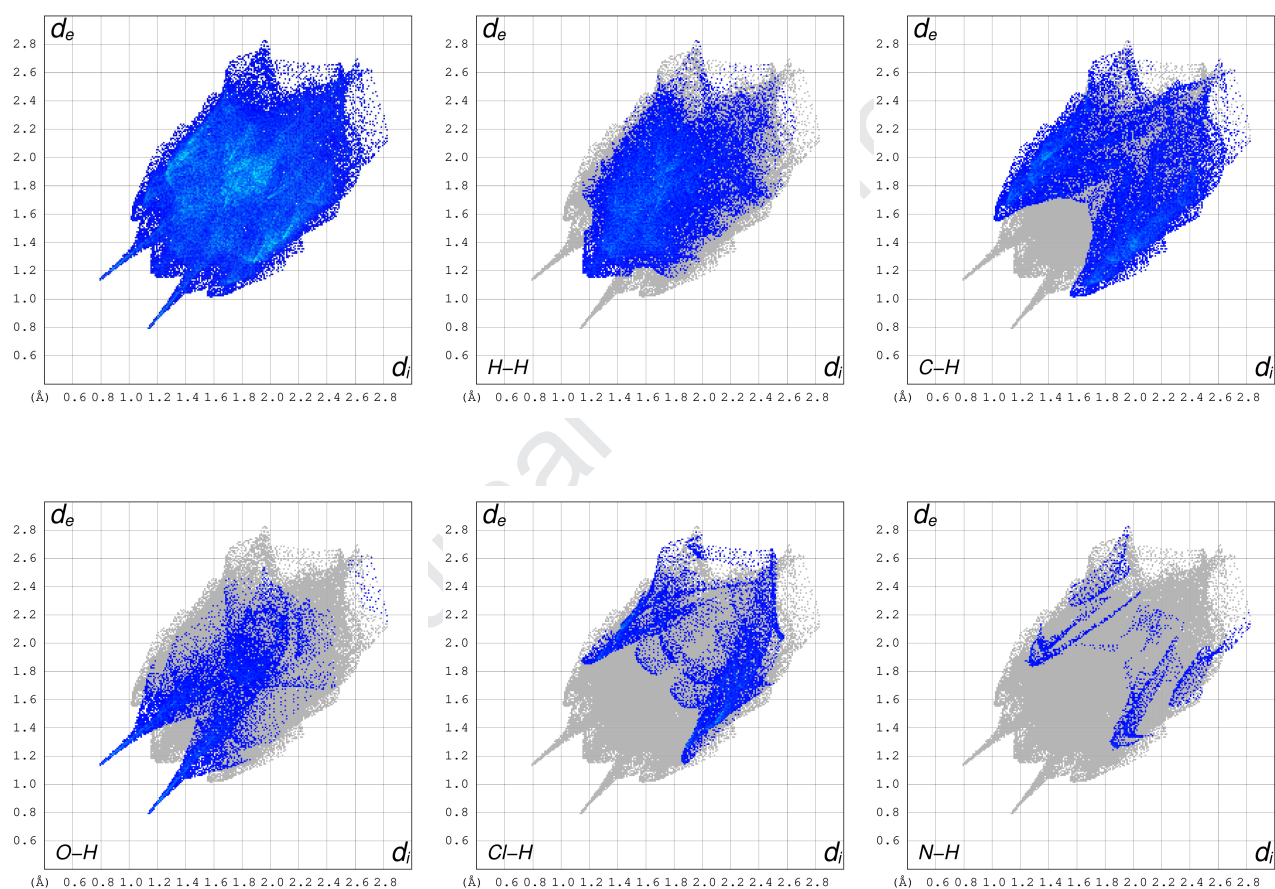


Figure 9: Fingerprint plots of the compound showing the contribution from all the contacts and resolved into individual contacts.

4.4.2 Shape index, curvedness, and electrostatic potential map

Shape index and curvedness are the two parameters which help to measure the surface curvature. Shape index is a dimensionless measure of ‘which shape’. For the two shapes, the shape index differs only by its sign which represents the complementary ‘stamp’ and ‘mould’ pairs. The shape index maps can be used to identify complementary hollows and bumps where two surfaces touch each other. The ‘bow tie’ patterns of red and blue triangles are characteristic of particular stacking arrangement of rings. The blue triangles represent the convex regions due to the ring carbon atoms of the molecule inside the surface, while the red triangles represent concave regions resulting from the carbon atoms of the π -stacked molecule above it.

Curvedness is a measure of ‘how much shape’. It is a function of the root-mean-square curvature of the surface. It is characterized by large green regions separated by dark blue edges. The flat surface in curvedness plot is an indication of planar stacking arrangements of the molecules.

Electrostatic potential mapping on Hirshfeld surface highlights electrostatic the complementarity between the adjacent molecules. The blue and red colored regions on the map are an indication of the hydrogen bond donors (electropositive) and acceptors (electronegative) regions respectively [50]. **Figures 10 (a), (b), and (c)** display the Hirshfeld surface mapped with shape index, curvedness, and electrostatic potential.

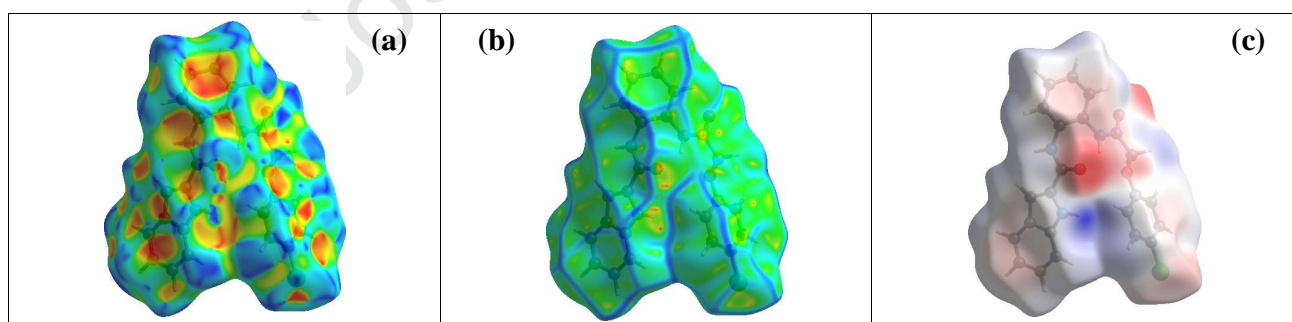


Figure 10 : Hirshfeld surface mapped with (a) shape index, (b) curvedness, and (c) electrostatic potential.

4.5. Energy frameworks

Energy frameworks play a vital role in the supramolecular assembly of molecules in the crystal. Using B3LYP/6-31G(d,p) hybrid functional basis set, energy frameworks were constructed using CrystalExplorer program. The cluster of molecular pairs involved in the interaction energy calculations are shown in **figure 11**. The 'R' in the figure represents the distance between the molecular centroids (mean atomic position) in Å. Different interaction energies, namely electrostatic, polarization, dispersion, and exchange repulsion, were calculated. The scale factors used for benchmarked energies are $k_{\text{ele}} = 1.057$, $k_{\text{pol}} = 0.740$, $k_{\text{disp}} = 0.871$, $k_{\text{rep}} = 0.618$ [51]. The graphical representation of Coulomb interaction energy (red), dispersion energy (green), total interaction energy (blue) of the compound viewed down *a*, *b*, and *c* axes are shown in **figure 12**. The cylinders in the framework show the relative strengths of molecular packing in different directions. The elimination of a few interaction energies below a certain value, to make the frames less crowded, results in less number of cylinders or the absence of cylinders in a particular direction.

The computed interaction energies for electrostatic, polarization, dispersion, and exchange repulsion are -178 kJ/mol, -42.7 kJ/mol, -310.7 kJ/mol, and 257 kJ/mol respectively. The dispersion energy dominates over other interaction energies.











	N	Symop	R	Electron Density	E_ele	E_pol	E_dis	E_rep	E_tot
	2	x, -y+1/2, z+1/2	9.47	B3LYP/6-31G(d,p)	-4.6	-0.7	-26.6	11.2	-21.6
	1	-x, -y, -z	10.79	B3LYP/6-31G(d,p)	0.3	-1.2	-17.3	5.2	-12.4
	2	-x, y+1/2, -z+1/2	13.38	B3LYP/6-31G(d,p)	-3.0	-0.4	-12.3	9.1	-8.5
	1	-x, -y, -z	7.71	B3LYP/6-31G(d,p)	-84.2	-22.7	-78.0	97.8	-113.3
	2	x, -y+1/2, z+1/2	14.45	B3LYP/6-31G(d,p)	0.6	-0.1	-1.6	0.0	-0.7
	2	x, y, z	9.31	B3LYP/6-31G(d,p)	-12.7	-2.9	-32.1	23.1	-29.3
	1	-x, -y, -z	5.12	B3LYP/6-31G(d,p)	-56.7	-12.4	-61.1	63.0	-83.5
	2	x, y, z	11.22	B3LYP/6-31G(d,p)	-1.9	-0.4	-6.4	2.3	-6.5
	1	-x, -y, -z	7.55	B3LYP/6-31G(d,p)	-15.1	-1.7	-66.4	38.1	-51.5
	2	-x, y+1/2, -z+1/2	11.53	B3LYP/6-31G(d,p)	-1.3	-0.2	-8.9	7.2	-4.9

Figure 11: The cluster of molecular pairs involved in the interaction energy calculations.

pairs involved in the interaction energy calculations.

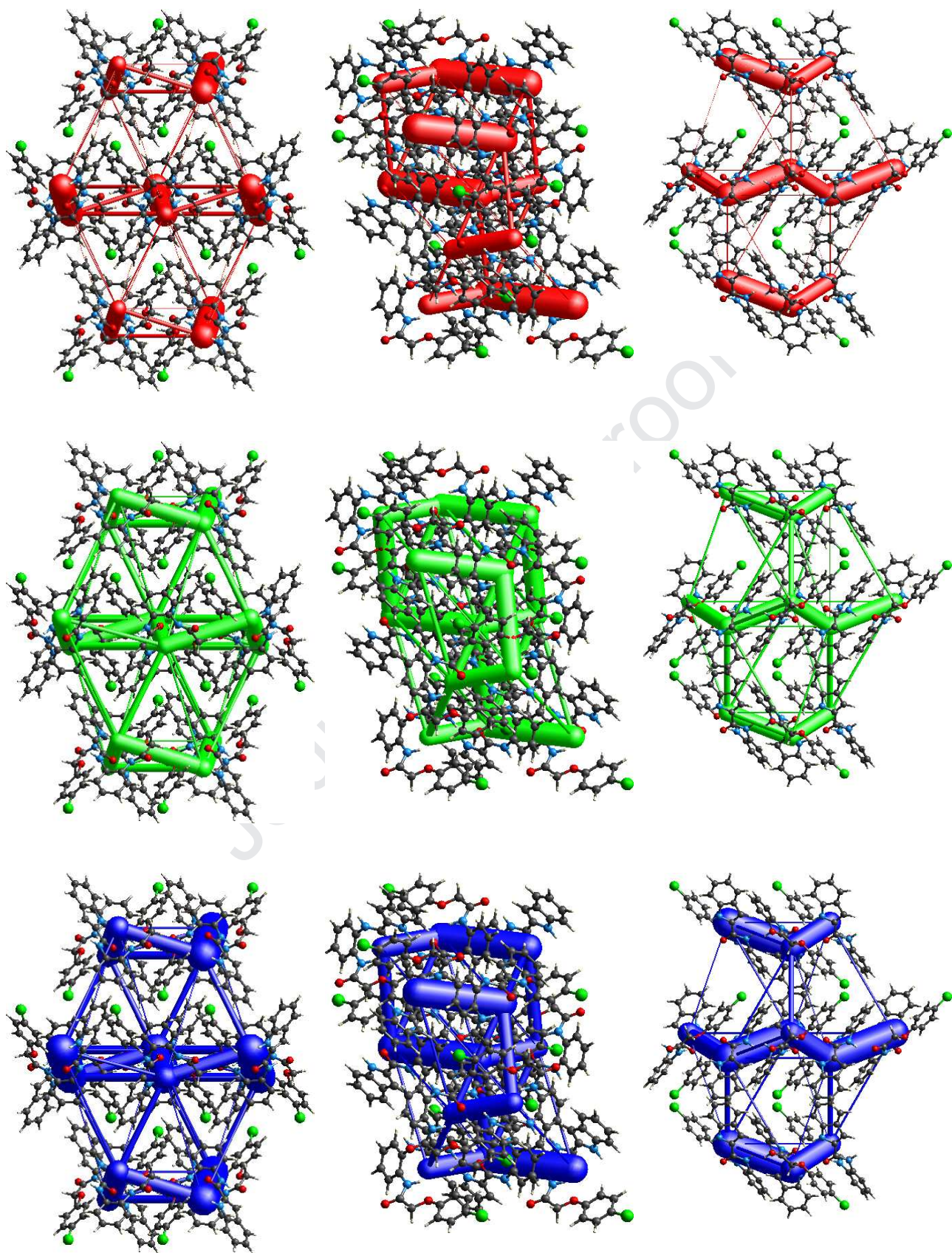


Figure 12 : The pictorial representation of Coulomb interaction energy (red), dispersion energy (green), total interaction energy (blue) of the compound viewed down *a*, *b*, and *c* axes respectively.

4. 6. AIM calculations

Atom in molecule theory calculations were performed to confirm the various intramolecular interactions which are responsible for the stability of the compound. Three different intramolecular interactions viz., C17-H17...O21, N19-H19...O11, and N19-H19...O23 were observed from XRD; but AIM calculations shows one additional intramolecular interaction C29-H29...O11 (**Figure 13**).

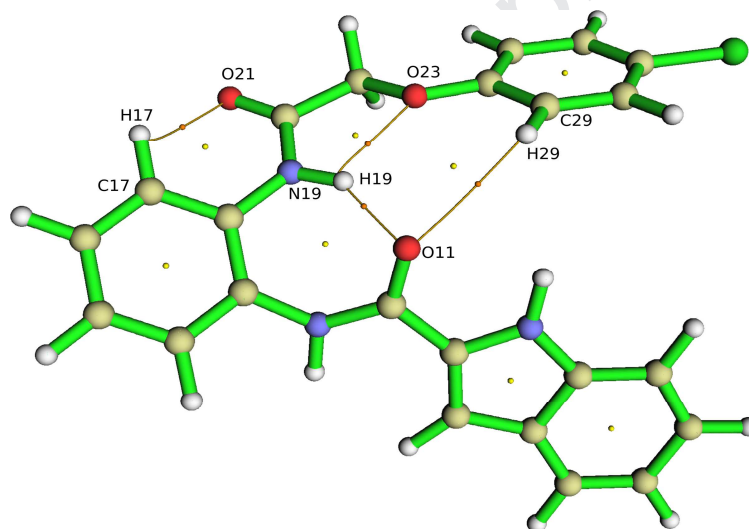


Figure 13: Molecule with intramolecular interactions from AIM calculations.

5.7 *In silico* validation

The Autodock program was utilized to produce the protein-tested compound-complex in order to understand the interaction between COX-1 & 2 proteins and ligand. It can be seen clearly that the ligand is placed at the center of the active site, and is stabilized by hydrogen bonding interactions. The hydrogen bonds exhibited in the COX-1 & 2 tested compound complexes have been documented together with their distances and angles, by taking into account the interaction energies of the tested compound with residues in the active site of the COX-1 & 2, key binding residues in the active site of

the model were determined and proved. It is obvious that the COX-1 & 2 tested compound complexes have a substantial binding energy of -7.87 and -6.77 kcal/mol, respectively. Also, it was shown by the interaction analysis that SER126 and PRO125, the amino acids residue of the COX-1 and HIS386 and GLN454, were the main providers for the inhibitory interaction (**figures 2 and 3**).

Conclusions

DFT calculations results showed the better agreement between the theoretical and experimental calculations. The orbital energy gap of 4.3267 eV between HOMO and LUMO, describes the partial hardness of the compound. Hirshfeld surface analysis was carried out to explore the intermolecular interactions. An approach to understand the packing of molecules in a crystal energy frameworks were constructed. The different interactions energies viz., electrostatic, dispersion, polarization, exchange repulsion between the molecular pairs were calculated; among these dispersion energy is dominant. The in silico study results confirmed that the title compound (5), has promising high active molecule for the inflammation treatment and good binding energy with exact pocket side to the specific protein. It is evident that the interaction energy of the compound (5) is lower in COX-1 as compared to COX-2 suggesting it to be a selective as a COX-1 inhibitor.

Acknowledgments

Fares Hezam Al-Ostoot is thankful to the government of Yemen and Al-Baydha University, Yemen, for providing financial assistance under the teacher's fellowship and University of Mysore, Mysuru, India. Geetha D. V. thanks UGC BSR for providing the fellowship. Yasser Hussein Eissa Mohammed is thankful to the University of Hajjah, Yemen. Shaukath Ara Khanum thankfully acknowledges the financial support provided by VGST, Bangalore, under CISEE Program [Project sanction order: No. VGST/CISEE/282].

References

- 1) Amin A. R., Vyas P., Attur M., Leszczynska-Piziak J., Patel I. R., Weissmann G., and Abramson S. B., The mode of action of aspirin-like drugs: Effect on inducible nitric oxide synthase, *Proceedings of the National Academy of Sciences USA*, 1995, 92, 7926–7930.

- 2) Shuttleworth S. J., Bailey S. G., and Townsend P. A., Histone deacetylase inhibitors: New promise in the treatment of immune and inflammatory diseases, *Current Drug Targets*, 2010, 11, 1430–1438.
- 3) Chattopadhyay M., Kodela R., Duvalsaint P. L., and Kashfi K., Gastrointestinal safety, chemotherapeutic potential and classic pharmacological profile of NOSH-naproxen (AVT-219) a dual NO- and H₂S-releasing hybrid, *Pharmacology Research & Perspectives*, 2016, 4, e00224.
- 4) Gierse J., Kurumbail R., Walker M., Hood B., Monahan J., Pawlitz J., Stegeman R., Stevens A., Kiefer J., Koboldt C., Mechanism of inhibition of novel COX-2 inhibitors, *Advances in Experimental Medicine and Biology*, 2002, 507, 365–369.
- 5) Amir M., and Kumar S., Anti-inflammatory and gastro sparing activity of some new indomethacin derivatives, *Archives of Pharmacal Research*, 2005, 338, 24–31.
- 6) Lal S., and Snape T. J., 2-Arylindoles: A privileged molecular scaffold with potent, broad-ranging pharmacological activity, *Current Medicinal Chemistry*, 2012, 19, 4828-4837.
- 7) Patel D. M., Sharma M. G., Vala R. M., Lagunes I, Puerta A, Padrón J. M., Rajani D. P., Patel H. M., Hydroxyl alkyl ammonium ionic liquid assisted green and one-pot regioselective access to functionalized pyrazolodihydropyridine core and their pharmacological evaluation, *Bioorganic Chemistry*, 2019, 86, 137-150.
- 8) Shimazaki Y., Yajima T., Takani M., and Yamauchi O., Metal complexes involving indole rings: structures and effects of metal–indole interactions, *Coordination Chemistry Reviews*, 2009, 253, 479-492.
- 9) Denhart D. J., Deskus J. A., Ditta J. L., Gao Q., King H. D., Kozlowski E. S., Meng Z., LaPaglia M. A., Mattson G. K., Molski T. S., Taber M. T., Lodge N. J., Mattson R. J., and Macor J. E., Conformationally restricted homotryptamines. Part 5: 3-(trans-2-aminomethylcyclopentyl) indoles as potent selective serotonin reuptake inhibitors, *Bioorganic & Medicinal Chemistry Letters*, 2009, 19, 4031-4033.
- 10) Sravanthi T. V., and Manju S. L., Indoles—a promising scaffold for drug development, *European Journal of Pharmaceutical Sciences*, 2016, 91, 1-10.
- 11) Ali S, Ali N, Ahmad D. B, Pradhan V, Farooqui M., Chemistry and biology of indoles and indazoles: a mini-review, *Mini reviews in medicinal chemistry*, 2013, 13, 1792-800.
- 12) Andreani A., Rambaldi M., Locatelli A., and Pifferi G., Synthesis and antiinflammatory activity of indolylacrylic and methylacrylic acids, *European Journal of Medicinal Chemistry*, 1994, 29, 903–906.

- 13) Sharma M. G. , Vala R. M., Patel D. M., Lagunes I, Fernandes M. X., Padrón J. M., Ramkumar V, Gardas R. L., Patel H. M., Anti-Proliferative 1, 4-Dihydropyridine and Pyridine Derivatives Synthesized through a Catalyst-Free, One-Pot Multi-Component Reaction, *Chemistry Select*, 2018, 43, 12163-12168.
- 14) Sharma M. G., Rajani D. P., Patel H. M., Green approach for synthesis of bioactive Hantzsch 1, 4-dihydropyridine derivatives based on thiophene moiety via multicomponent reaction, *Royal Society open science*, 2017, 6, 170006.
- 15) Mohamad Y. E. M., Lashine Sayed M., El-Adl Sobhy E., and Abou Kull Mansour, *Zagazig Journal of Pharmaceutical Science*, 1994, 3, 40–48.
- 16) Kumar A., Saxena K. K., Gurtu S., Sinha J. N., and Shanker K., Indole alkaloids have been proved to be medicinally important natural drug, *Indian Drugs*, 1986, 24, 1–5.
- 17) Suzen S., and Büyükbingöl E., Anti-cancer activity studies of indolalithiohydantoin (PIT) on certain cancer cell lines, *Il Farmaco*, 2000, 55, 246-248.
- 18) Büyükbingöl E., Süzen S., and Klopman G., Studies on the synthesis and structure-activity relationships of 5-(3'-indolal)-2-thiohydantoin derivatives as aldose reductase enzyme inhibitors, *Farmaco (SocietÃ chimica italiana:1989)*, 1994, 49, 443-447.
- 19) Suzen S., and Buyukbingol E., Evaluation of anti-HIV activity of 5-(2-phenyl-3'-indolal)-2-thiohydantoin, *Il Farmaco*, 1998, 53, 525-527.
- 20) Abdelrahman M. H., Aboraia S. A., Youssif B. G. M., and Elsadek B. E. M., Design, synthesis and pharmacophoric model building of new 3-alkoxymethyl/3-phenyl indole-2-carboxamides with potential antiproliferative activity, *Chemical Biology & Drug Design*, 2017, 90, 64-82.
- 21) Megna B. W., Carney P. R., Nukaya M., Geiger P., and Kennedy G. D., Indole-3-carbinol induces tumor cell death: Function follows form, *Journal of Surgical Research*, 2016, 204, 47-54.
- 22) Mohammed, Y. H. E., Malojirao V. H., Thirusangu P., Al-Ghorbani M., Prabhakar B. T., and Shaukath A. K., The Novel 4-Phenyl-2-Phenoxyacetamide Thiazoles modulates the tumor hypoxia leading to the crackdown of neoangiogenesis and evoking the cell death, *European Journal of Medicinal Chemistry*, 2018, 143, 1826-1839.

- 23) Azizmohammadi M., Khoobi M., Ramazani A., Saeed E., Abdolhossein Z., Omidreza F., Ramin M., and Abbas S., 2H-chromene derivatives bearing thiazolidine-2, 4-dione, rhodanine or hydantoin moieties as potential anticancer agents, *European Journal of Medicinal Chemistry*, 2013, 59, 15-22.
- 24) Liebmann P. M., Albert W., Peter F., Dietmar H., and Konrad S., Melatonin and the immune system, *International Archives of Allergy and Immunology*, 1997, 112, 203-211.
- 25) Pagé D., Yang H., Brown W., Walpole C., Fleurent M., Fyfe M., Gaudreault F., and St-Onge S., New 1, 2, 3, 4-tetrahydropyrrolo [3, 4-b] indole derivatives as selective CB2 receptor agonists. *Bioorganic & Medicinal Chemistry Letters*, 2007, 17, 6183-6187.
- 26) Yau-Jan C., Poeggeler B., Omar R. A., Chain D. G., Frangione B., Ghiso J., and Pappolla M. A., Potent neuroprotective properties against the Alzheimer β -amyloid by an endogenous melatonin-related indole structure, indole-3-propionic acid, *Journal of Biological Chemistry*, 1999, 274, 21937-21942.
- 27) (a) Choudhary A. N., Kumar A., Joshi A., and Kohli M. S., Synthesis of tryptoline-3-carboxylic acid derivatives a novel antidiabetic agent, *Journal of Young Pharmacists*, 2011, 3, 132-137. (b) Naureen, Sadia, Shazia Noreen, Areesha Nazeer, Muhammad Ashraf, UMBER Alam, MunawarAli Munawar, and Misbahul Ain Khan. Triarylimidazoles-synthesis of 3-(4, 5-diaryl-1H-imidazol-2-yl)-2-phenyl-1H-indole derivatives as potent α -glucosidase inhibitors, *Medicinal Chemistry Research*, 2015, 24, 1586-1595.
- 28) (a) Bandini, Marco, Alfonso Melloni, and Achille Umani-Ronchi. New catalytic approaches in the stereoselective Friedel-Crafts alkylation reaction, *Angewandte Chemie International Edition*, 2004, 43, 550-556. (b) Austin, Joel F., and David W. C. M., Enantioselective organocatalytic indole alkylations. Design of a new and highly effective chiral amine for iminium catalysis, *Journal of the American Chemical Society*, 2002, 124, 1172-1173.
- 29) (a) Srivastava N. and Banik B. K. Bismuth nitrate-catalyzed versatile Michael reactions, *The Journal of organic chemistry*, 2003, 68, 2109-2114. (b) Bartoli G., Bartolacci M., Bosco M., Foglia, Giuliani A., Marcantoni E., Sambri L., and Torregiani E., The Michael Addition of Indoles to α , β -Unsaturated Ketones Catalyzed by $\text{CdCl}_2 \cdot 7\text{H}_2\text{O}$ -NaI Combination Supported on Silica Gel, *The Journal of Organic Chemistry*, 2003, 68, 4594-4597.
- 30) Nagaraja N., Sharath V., and Vijay Kumar H., Novel indole-2-carboxylic acid analogues: Synthesis and a new light in to their antioxidant potentials, *European Journal of Chemistry*, 2012, 3, 214-219.

- 31) Geetha D. V., Fares Hezam A., Yasser Hussein E. M., Sridhar M. A., Shaukath A. K., and Lokanath N. K., Synthesis, Elucidation, Hirshfeld surface analysis, and DFT calculations of 4-chloro-N-[2-(2-1H-indol-3-yl-acetylamino)-phenyl]-benzamide, *Journal of Molecular Structure*, 2019, 1178, 384-393.
- 32) Gopal S., Sumati A., Geetha D. V., Fares Hezam A., Yasser Hussein E. M., Shaukath A. K., Sridhar M. A., and Rajni Kant, Synthesis, structure and molecular docking analysis of an anticancer drug of N-(2-aminophenyl)-2(2-isopropylphenoxy) acetamide. *Molecular Crystals and Liquid Crystals*. 2019, 675(1), 85-95.
- 33) Karthik K., Fares Hezam A., Yasser Hussein E. M., Shaukath A. K., and Lokanath N. K., Synthesis, crystal structure and 3D energy frameworks of ethyl 2-[5-nitro-2-oxopyridine-1(2H)-yl] acetate: Hirshfeld surface analysis and DFT calculations. *Chemical Data Collections*. 2019, 20, 100195.
- 34) Madan S. K., Fares Hezam A., Manjunath B. C., Shamprasad V. R., Mohammed Y. H., Mahesh N., Shaukath A. K., Lokanath N. K., and Byrappa K., Crystal packing analysis of 1-(3, 4-dimethoxyphenyl)-3-(4-bromophenyl) prop-2-en-1-one exhibiting a putative halogen bond C-Br...O., *Journal of Molecular Structure*, 2018, 1156, 216-223.
- 35) Neralagundi H. G., Shamanth A., Bushra Begum B. T., Prabhakar, and Shaukath A. K., Design and synthesis of diamide-coupled benzophenones as potential anticancer agents, *European Journal of Medicinal Chemistry*, 2016, 115, 342-351.
- 36) Madan S. K., Manjunath B. C., Fares Hezam A. H., Jyothi M., Al-Ghorbani M., Shaukath A. K., Avinash K. K., Lokanath N. K., and Byrappa K., Synthesis, crystal structure and Hirshfeld surfaces of 1-(3, 4-dimethoxyphenyl)-3-(3-hydroxyphenyl) prop-2-en-1-one, *Chemical Data Collections*, 2018, 15, 153-160.
- 37) Fares Hezam A., Yasser Hussein E. M., Zabiulla M., Kempaiah A. N., Shaukath A. K., Synthesis, in silico study and in vitro antimicrobial evaluation of some new N-benzoyl-N'-[2-(4chloro-phenoxy)-acetyl]-hydrazides analogs, *Journal of Applied Pharmaceutical Science*, 2019, 9, 042-049.
- 38) Schmidt M. W., Baldrige K. K., Boatz J. A., Elbert S. T., Gordon M. S., Jensen J. H., Koseki S., Matsunaga N., Nguyen K. A., Su S. J., Windus T. L., Dupuis M., Montgomery J. A., General Atomic and Molecular Electronic Structure System, *Journal of Computational Chemistry*, 1993, 14, 1347-1363.
- 39) Becke A. D., Density-functional thermochemistry. III. The role of exact exchange, *The Journal of Chemical Physics*, 1993, 98, 5648-5652.

- 40) Patel H. M., Rajani D. P., Sharma M. G., Bhatt H. G., Synthesis, Molecular Docking and Biological Evaluation of Mannich Products Based on Thiophene Nucleus using Ionic Liquid. *Letters in Drug Design & Discovery*, 2019, 16, 119-126.
- 41) Patel H. M., Patel K. D., Patel H. D., Facile synthesis and biological evaluation of New Mannich products as potential antibacterial, antifungal and antituberculosis agents: molecular docking study, *Current Bioactive Compounds*, 2017, 13, 47-58.
- 42) Fani N., Bordbar A. K., Ghayeb Y., Spectroscopic, docking and molecular dynamics simulation studies on the interaction of two Schiff base complexes with human serum albumin, *Journal of Luminescence*, 2013, 141, 166-172.
- 43) Lee C., Yang W., and Parr R. G., Development of the Colic-Salvetti correlation-energy formula into a functional of the electron density, *Physical Review B*, 1988, 37(2). 785-789.
- 44) Lu T., and Chen F., Multiwfn: A multifunctional wavefunctional analyzer, *Journal of Computational Chemistry*, 2012, 33, 580-592.
- 45) Sandeep G., Nagasree K. P., Hanisha M. M., and Kumar M. M. K., AUdocker L. E: A GUI for virtual screening with AUTODOCK Vina. *BMC Research Notes*. 2011, 4, 445.
- 46) Zabiulla Z., Malojirao V. H., Mohammed Y. H., Thirusangu P., Prabhakar B. T., Khanum S. A., Synthesis, molecular docking, and apoptogenic efficacy of novel N-heterocycle analogs to target B-cell lymphoma 2/X-linked inhibitors of apoptosis proteins to regress melanoma, *Medicinal Chemistry Research*, 2019, 28, 1132–1160.
- 47) McKinnon J. J., Spackman M. A., and Mitchell A. S., Novel tools for visualizing and exploring intermolecular interactions in molecular crystals, *Acta Crystallographica Section B: Structural Science*, 2004, 60, 627-668.
- 48) Khamees H. A., Mohammed Y. H., Ananda S., Fares Hazem A., Sangappa Y., Alghamdi S, Khanum S. A., Mahendra M., Effect of o-difluoro and p-methyl substituents on the structure, optical properties and anti-inflammatory activity of phenoxy thiazole acetamide derivatives: Theoretical and experimental studies, *Journal of Molecular Structure*, 2019, 6, 127024.
- 49) McKinnon J. J., Jayatilaka D., and Spackman M. A., Towards quantitative analysis of intermolecular interactions with Hirshfeld surfaces, *Chemical Communications*, 2007, 37, 3814–3816.
- 50) Harsh Y., Nidhi S., and Binay K., Growth and characterization of piezoelectric benzil single crystals and its application in microstrip patch antenna, *Crystal Engineering Communication*, 2014, 16, 10700-10710.

- 51) Turner M. J., Grabowsky S., Jayatilaka D., and Spackman M. A., Accurate and efficient model energies for exploring intermolecular interactions in molecular crystals, *The Journal of Physical Chemistry Letters*, 2014, 24, 4249-4255.

Journal Pre-proof

Highlights

- . The article describes the synthesis, characterization, molecular docking, and computational studies of the compound.
- . Hirshfeld surface analysis, interaction energies, and energy frameworks are studied in detail.
- . DFT calculations are performed to optimize the molecular geometry using B3LYP functional with 6-31 G(d,p) and 6-31+G (d, p) as basis sets.
- . HOMO, LUMO frontier molecular orbitals are analyzed.
- . The molecular docking of an anti-inflammatory drug was carried out.